

On the Eccentricity Distribution of Short-Period Single-Planet Systems

Ji Wang¹ and Eric B. Ford¹★

¹*Department of Astronomy, University of Florida, 211 Bryant Space Science Center, Gainesville, FL, USA, 32611*

23 October 2018

ABSTRACT

We apply standard Markov chain Monte Carlo (MCMC) analysis techniques for 50 short-period, single-planet systems discovered with radial velocity technique. We develop a new method for accessing the significance of a non-zero orbital eccentricity, namely Γ analysis, which combines frequentist bootstrap approach with Bayesian analysis of each simulated data set. We find the eccentricity estimations from Γ analysis are generally consistent with results from both standard MCMC analysis and previous references. The Γ method is particularly useful for assessing the significance of small eccentricities. Our results suggest that the current sample size is insufficient to draw robust conclusions about the roles of tidal interaction and perturbations in shaping the eccentricity distribution of short-period single-planet systems. We use a Bayesian population analysis to show that a mixture of analytical distributions is a good approximation of the underlying eccentricity distribution. For short-period planets, we find the most probable values of parameters in the analytical functions given the observed eccentricities. These analytical functions can be used in theoretical investigations or as priors for the eccentricity distribution when analyzing short-period planets. As the measurement precision improves and sample size increases, the method can be applied to more complex parametrizations for the underlying distribution of eccentricity for extrasolar planetary systems.

Key words: methods: statistical-planetary systems-techniques: radial velocity.

1 INTRODUCTION

The discovery of exoplanets has significantly advanced our understanding of formation and evolution of planetary system (Wolszczan 1994; Mayor & Queloz 1995; Marcy & Butler 1996). As of February 2011, over 500 exoplanets have been discovered including 410 systems detected by radial velocity (RV) technique¹. The eccentricity distribution of exoplanets is very different from that of solar system. For sufficiently short-period planets, it is expected that tidal circularization would lead to nearly circular orbits. Yet, several short-period planets appear to have eccentric orbits. Several mechanisms (e.g. planet scattering, Kozai effect) have been proposed to explain the observed eccentricity distribution (Takeda & Rasio 2005; Zhou & Lin 2007; Ford & Rasio 2008; Jurić & Tremaine 2008). This paper aims to improve our understanding of the true eccentricity distribution and its implications for orbital evolution.

The Bayesian approach offers a rigorous basis for determining the posterior eccentricity distribution for individual system. The Bayesian method is particularly advantageous relative to traditional bootstrap method when the orbital eccentricity is poorly

constrained by RV data (Ford 2006). Ford (2006) discussed eccentricity estimation using Markov Chain Monte Carlo (MCMC) simulation in the framework of Bayesian inference theory and found a parameter set that accelerates convergence of MCMC for low eccentricity orbit. For a population of planets on nearly circular orbits, eccentricity estimates for planets on circular orbit are biased resulting in overestimation of orbital eccentricities (Zakamska et al. 2011). Further complicating matters, the population of known exoplanets is not homogeneous, and the observed eccentricity distribution is affected by the discovery method, selection effects and data analysis technique.

In this paper, we construct a catalog of short-period single-planet systems using homogeneous RV data reduction process, i.e., standard MCMC analysis (§2.1). In §2.2, we describe a new method of estimating Keplerian orbital parameters, namely Γ analysis. We present the results for standard MCMC analysis in §3. We compare the results of both methods with each other and the results from previous references. We interpret the results to investigate how tidal effect and perturbation affect the orbital eccentricity distribution of short-period planets (§4). In §5, we provide an analytical function for the underlying eccentricity distribution that is able to reproduce the observed the eccentricity distribution. We discuss the results in §6 and summarize our conclusions in §7.

★ E-mail: jwang@astro.ufl.edu (JW); eford@astro.ufl.edu (EBF)

¹ <http://exoplanet.eu/>; <http://exoplanets.org>

2 METHOD

We select all the systems with: 1) a single known planet discovered with the radial velocity technique as of April 2010; 2) an orbital period of less than 50 days; and 3) a publicly available radial velocity data set. We exclude planets discovered by the transit technique in order to avoid complications due to selection effects (Gaudi et al. 2005). We perform an orbital analysis on each system in our sample using: 1) a standard MCMC analysis (§2.1) and 2) a new method, Γ analysis (described in §2.2). We focus on the eccentricity estimation for each planet since the eccentricity is an important indication of orbital evolution and tidal interaction.

2.1 Bayesian Orbital Analysis of Individual Planet

We performed a Bayesian analysis of the published radial velocity observation using a model consisting of one low-mass companion following a Keplerian orbit. If a long-term RV trend is included in the original paper reporting the RV data or if a linear trend of more than $1 \text{ m} \cdot \text{s}^{-1} \cdot \text{yr}^{-1}$ is apparent, then we add to the model a constant long-term acceleration due to distant planetary or stellar companion.

We calculate a posterior sample using the Markov Chain Monte Carlo (MCMC) technique as described in Ford (2006). Each state in the Markov chain is described by the parameter set $\vec{\theta} = \{P, K, e, \omega, M_0, C_i, D, \sigma_j\}$, where P is orbital period, K is the velocity semi-amplitude, e is the orbital eccentricity, ω is the argument of periastron, M_0 is the mean anomaly at chosen epoch τ , C_i is constant velocity offset (subscript i indicates constant for different observatory), D is the slope of a long-term linear velocity trend, and σ_j is the ‘‘jitter’’ parameter. The jitter parameter describes any additional noise including both astrophysical noises, e.g., stellar oscillation, stellar spots (Wright et al. 2005) and any instrument noise not accounted for in the reported measurement uncertainties. The RV perturbation of a host star at time t_k due to a planet on Keplerian orbit and possible perturbation is given by

$$v_{k,\vec{\theta}} = K \cdot [\cos(\omega + T) + e \cdot \cos(\omega)] + D \cdot (t_k - \tau), \quad (1)$$

where T is the true anomaly which is related to eccentric anomaly E via the relation,

$$\tan\left(\frac{T}{2}\right) = \sqrt{\frac{1+e}{1-e}} \tan\left(\frac{E}{2}\right). \quad (2)$$

The eccentric anomaly is related to the mean anomaly M via Kepler’s equation,

$$E(t) - e \cdot \sin[E(t)] = M(t) - M_0 = \frac{2\pi}{P}(t - \tau). \quad (3)$$

We choose priors of each parameter as described in Ford & Gregory (2007). The prior is uniform in logarithm of orbital period. For K and σ_j we use a modified Jefferys prior in the form of $p(x) \propto (x + x_0)^{-1}$ (Gregory 2005) with $K_{\min} = 0.1 \text{ m} \cdot \text{s}^{-1}$. Priors are uniform for: e ($0 \leq e \leq 1$), ω and M ($0 \leq \omega, M < 2\pi$), C_i and D . We verified that the parameters in $\vec{\theta}$ did not approach the limiting values. We assume each observation results in a measurement drawn from normal distribution centered at the true velocity, resulting in a likelihood (i.e., conditional probability of making the specified measurements given a particular set of model parameters) of

$$p(\vec{v}|\vec{\theta}, M) \propto \prod_k \frac{\exp[-(v_{k,\vec{\theta}} - v_k)^2 / 2\sigma_k^2]}{\sigma_k}, \quad (4)$$

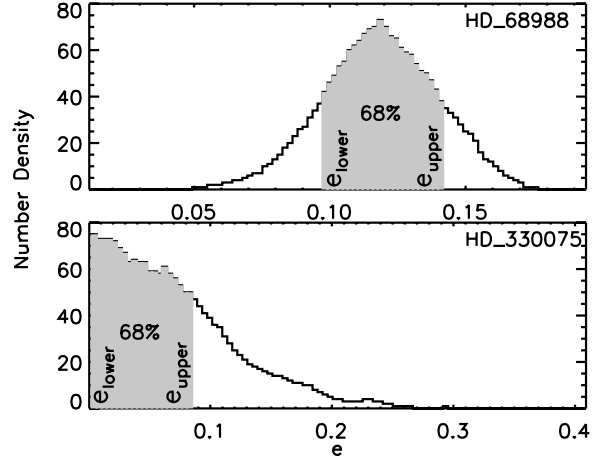


Figure 1. Examples of how credible intervals of standard MCMC analysis are calculated using posterior distribution of e . Grey region contains 68% of total number of posterior samples of e .

where v_k is radial velocity at time t_k , and $v_{k,\theta}$ is the model velocity at time t_k given the model parameters $\vec{\theta}$. Noise σ_k consists of two parts. One component is from the observation uncertainty $\sigma_{k,obs}$ reported in the radial velocity data, and the other is the jitter, σ_j , which accounts for any unforeseen additional noise including instrument instability and stellar jitter. The two parts are added in quadrature in order to generate σ_k . We calculate the Gelman-Rubin statistic, \hat{R} , to test for nonconvergence of Markov chains.

We perform a MCMC analysis for RV data set of each system in the sample and obtain posterior samples of h and k , where $h = e \cos \omega$ and $k = e \sin \omega$. This parameterization has been shown to be more effective in description of the eccentricity distribution for low eccentric orbits (Ford 2006). We take steps in h and k and adjust the acceptance rate according to the Jacobian of the coordinate transformation, so as to maintain a prior that is uniform in e and ω . Mean values, \bar{h} and \bar{k} , from posterior samples of h and k are adopted to calculate e_{MCMC} using the equation $e_{MCMC} = \sqrt{\bar{h}^2 + \bar{k}^2}$. The posterior distribution of e is not always Gaussian distribution especially near $e \sim 0$. Therefore, it is not appropriate to calculate the uncertainty of e using the equation of error propagation in which gaussian noise is assumed. We use posterior distribution of e to infer the credible interval of e . The boundaries of the region where 68% posterior samples populate are adopted as e_{lower} and e_{upper} (Appendix A1). Fig. 1 illustrates two examples of how the credible intervals are inferred for HD 68988 (eccentric orbit) and HD 330075 (circular orbit).

2.2 Γ Analysis of Individual Systems

A fully Bayesian analysis of the population of exoplanet eccentricities would be computationally prohibitive due to the large number of dimensions. Therefore, we develop a hybrid Bayesian-frequentist method to evaluate the significance of a non-zero eccentricity measurement. We combine a bootstrap style approach of generating and analyzing synthetic data sets with MCMC analysis of each synthetic data set to obtain a frequentist confidence level for each eccentricity that accounts for biases. First, we perform the standard MCMC analysis described in §2.1 on the real RV data set and adopt the mean value of each orbital parameter in $\vec{\theta}$ except e . We generate a series of simulated radial velocity data sets

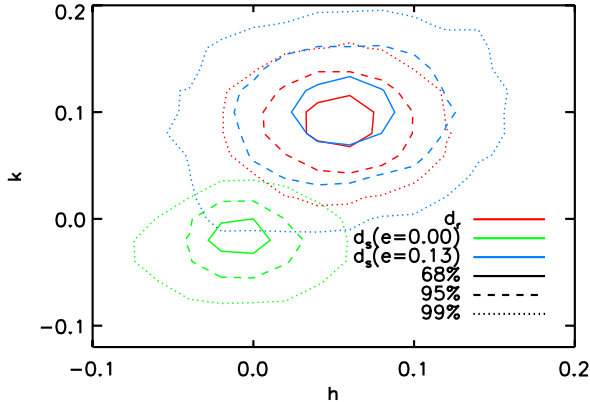


Figure 2. Contours of posterior distribution in h and k space for HD 68988 (Solid-68% of sample points included; dashed-95% of sample points included; dotted-99% of sample points included). Red contours are posterior distribution for real observation, green contours are for simulated RV data set with $e=0.00$, and blue contours are for simulated RV data set with $e=0.13$. Eccentricity of HD 68988 is 0.1250 ± 0.0087 according to Butler et al. (2006).

at different values of e . The adopted K is scaled accordingly to $K \propto (1 - e^2)^{-0.5}$. The simulated radial velocity data has the same number of observations, and each simulated observation takes place at exactly the same time and the same mean anomaly as the real observation. Gaussian noise with standard deviation of σ_k (§2.1) are added to simulated radial velocity data sets at different eccentricities. Each simulated RV data set has the same reported RV measurement uncertainties as the real RV observations. Standard MCMC analysis is then performed on each of the simulated RV data sets.

For both real and simulated data sets, we construct a two-dimensional histogram using the posterior samples in (h, k) space to approximate a two-dimensional posterior distribution for h and k , $d_r(h_i, k_j)$ and $d_s(h_i, k_j)$, where i and j denote bin indices, and the subscripts r and s denote the real and simulated data set. We compare the distribution for each simulated data set $d_s(h_i, k_j)$ to the distribution for real radial velocity data set $d_r(h_i, k_j)$. To quantify the similarity between $d_s(h_i, k_j)$ and $d_r(h_i, k_j)$, we calculate the statistic defined as $\Gamma = [\sum_{i=1}^N \sum_{j=1}^N (d_s(h_i, k_j) - \mu_s) \cdot (d_r(h_i, k_j) - \mu_r)] / [\sigma_s \sigma_r (N^2 - 1)]$, where N is the number of bins in h or k dimension, μ and σ represent mean and standard deviation. In other words, the Γ statistic is obtained by cross-correlating two posterior distributions in h and k space. Fig 2 illustrates the process by which we obtain Γ for the case of HD 68988. If $d_s(h_i, k_j)$ matches $d_r(h_i, k_j)$, we expect to obtain a Γ value that approaches unity (blue and red contours). If the samples differ significantly then Γ decreases towards zero (red and green contours). For each eccentricity, we simulated 21 radial velocity data sets and compare $d_s(h_i, k_j)$ with $d_r(h_i, k_j)$ to obtain 21 Γ statistics between simulated and real RV data. We choose the median value $\bar{\Gamma}$ as an indicator of overall similarity at given eccentricity.

Based on above analysis of simulated radial velocity data with different input eccentricities e , we obtain a relationship between $\bar{\Gamma}$ and e , i.e. $\bar{\Gamma}(e)$. We use a high-order polynomial to interpolate for $\bar{\Gamma}(e)$. We define \bar{e} to be the eccentricity at which $\bar{\Gamma}(e)$ reaches maximum and we interpret \bar{e} as an estimator of eccentricity. For HD 68988 (Fig. 3), input eccentricity ranges from 0.00 to 0.29 with step size of 0.01. $\bar{\Gamma}(e)$ reaches maximum at $e = 0.134$. We estimate

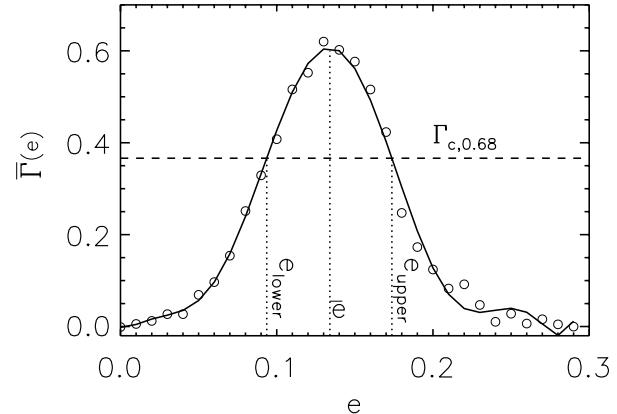


Figure 3. $\bar{\Gamma}$ as a function of eccentricity e for HD 68988. Open circles are results from simulations, solid line is the result of polynomial fitting. The long dashed line is the critical threshold, $\Gamma_{c,0.68}$ at the 68% confidence level.

statistical confidence level of \bar{e} using every pair of posterior eccentricity samples calculated from the data sets that are generated assuming the same eccentricity. Consider the example of HD 68988 again: 21 sets of posterior distribution in h and k space, $d_s(h_i, k_j)$, are obtained. Comparison between each pair gives a Γ statistic between simulated RV data. $\sum_{i=1}^{20} = 210$ Γ statistics in total for simulated RV data sets are calculated at eccentricity of 0.13 and 68.1% of pairs (143 out of 210) have a Γ statistic greater than 0.3714. We define this value, $\Gamma_{c,0.68}$, as the critical Γ value for HD 68988 at 68% confidence level for $e = 0.13$. Therefore, if Γ statistic obtained in comparison between $d_s(h_i, k_j)$ and $d_r(h_i, k_j)$ is less than $\Gamma_{c,0.68}$, we argue that the eccentricity inferred from simulated RV data set is not consistent with the observed eccentricity of the system at 68% confidence level. In the case where \bar{e} is located between grids of simulated e values, we calculate $\Gamma_{c,0.68}$ at \bar{e} using interpolation of $\Gamma_{c,0.68}$ at nearby e values. We use a high-order polynomial to approximate the discrete data $\bar{\Gamma}(e)$. The polynomial is later used to infer \bar{e} , lower and upper limit of eccentricity. For HD 68988, $\Gamma_{c,0.68}$ is 0.3663 at $\bar{e} = 0.134$ after interpolation. Using the relationship between $\bar{\Gamma}$ and e (Fig. 3), we look for the e values corresponding to $\Gamma_{c,0.68}$ as estimators of the lower and upper limit for eccentricity of the planet system at a 68% confidence level. In HD 68988, we obtained $e = 0.134^{+0.040}_{-0.040}$ using Γ analysis. In comparison, we have obtained $e = 0.119^{+0.025}_{-0.022}$ using a standard MCMC analysis and Butler et al. (2006) reported $e = 0.125 \pm 0.009$.

3 RESULTS FOR INDIVIDUAL PLANETS

In our sample of 50 short-period single-planet systems, we successfully analyzed 42 systems using Γ analysis, and 46 systems using standard MCMC analysis (Appendix A1). All the error are based on a 68% confidence level (Γ analysis) or a 68% credible interval (MCMC). The unsuccessful cases in standard MCMC analysis are HD 189733, HD 219828, HD 102195 and GJ 176. In HD 189733, most of the RV data points were taken during observation of Rossiter-McLaughlin effect, which is not modeled here. MCMC analysis fails for HD 219828 and GJ 176 because of low signal to noise ratio ($K=7 \text{ m} \cdot \text{s}^{-1}$ and $n_{obs}=20$ for HD 219828 and $K=4.1 \text{ m} \cdot \text{s}^{-1}$ and $n_{obs}=57$ for GJ 176). RV data points of HD 102195 were taken at 3 observatories and MCMC analysis is complicated

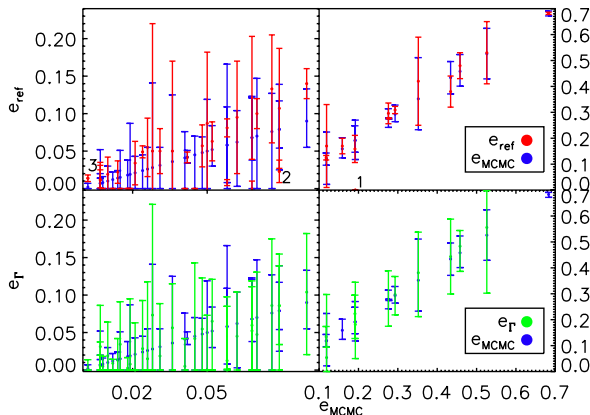


Figure 4. Top: comparison between standard MCMC analysis (blue) and previous references (red); Bottom: comparison between standard MCMC analysis (blue) and Γ analysis (green). The systems where disagreements take place are marked with a number: 1, HD 149026; 2, τ Boo; 3, HD 195019.

using different observatory offsets. In addition to the above, Γ analysis was unsuccessful for HD 162020, GJ 86, HD 17156 and HD 6434. Since Γ analysis involves generating simulated RV data, the limited number of observations and partial phase coverage for these systems can cause poor convergence for some simulated data sets. These limitations become more severe for systems with high eccentricity (e.g. HD 17156, $e = 0.684$) since phase coverage is more important for eccentric orbits.

3.1 Comparison: Standard MCMC and References

In Fig. 4 (top), we compare results from two sources, standard MCMC analysis and previous references. In most cases the two methods provide similar results. We found there are 3 systems for which the eccentricity estimates are not consistent, i.e., the published eccentricity error bar does not overlap the 68% credible interval from our MCMC analysis. They are HD 149026, τ Boo, HD 195019. For HD 149026, Sato et al. (2005) set the eccentricity to be zero when fitting the orbit. In contrast, we treat eccentricity as a variable and the standard MCMC method found that the 68% credible interval for the systems mentioned above does not include zero. In addition, HD 149026 b is a known transiting planet and transit photometry provides additional constraints on eccentricity which we have not included (Charbonneau 2003). Knutson et al. (2009) measured $\Delta t_{\Pi} = 20.9^{+7.2}_{-6.2}$ minute (2.9σ) for HD 149026 which is inconsistent with zero eccentricity, because $e \geq e \cos \omega \approx \frac{\pi}{2P} \Delta t_{\Pi}$, where P is period and Δt_{Π} is the deviation of secondary eclipse from midpoint of primary transits. Standard MCMC results for other two systems (τ Boo and HD 195019) are not consistent with those from previous references even though eccentricity was treated as variable in previous references. Butler et al. (2006) report $e = 0.023 \pm 0.015$ for τ Boo and $e = 0.014 \pm 0.004$ for HD 195019. On the contrary, standard MCMC analysis gives $e = 0.0787^{+0.0382}_{-0.0246}$ for τ Boo and $e = 0.0017^{+0.0049}_{-0.0017}$ for HD 195019 (See Appendix A1).

3.2 Comparison: Standard MCMC and Γ Analysis

Fig. 4 (bottom) compares the results from standard MCMC analysis and Γ analysis. We find that the 68% credible/confidence intervals for the two methods overlap in the cases where there are

discrepancies between standard MCMC analysis and previous references (see § 3.1). The confidence interval from the Γ analysis is generally larger than the credible interval from a standard MCMC analysis. The larger uncertainty from Γ analysis is likely due to the analysis accounting for the uncertainty in each velocity observation twice, first when generating synthetic data sets and a second time when analyzing the simulated data. Thus, the Γ analysis results in slightly larger uncertainty in eccentricity estimation.

In order to understand the behavior of standard MCMC analysis and Γ analysis for planets on nearly circular orbits, we conduct an additional experiment generating many synthetic data sets where each system has a single planet on a circular orbit. We assume that they are observed at the same times and with the same RV measurement precisions as actual RV data sets. In order to understand the bias of each method for nearly circular systems, we compare the output eccentricities and their uncertainties. Using standard MCMC analysis, we find that $76.4 \pm 2.9\%$ of the simulated data sets are consistent with zero using a 68% credible interval, and $23.6 \pm 1.6\%$ of the simulated data sets have 68% credible intervals that do not include zero. In contrast, for $16.8 \pm 1.4\%$ of the simulated data sets, the Γ analysis does not result in a 68% confidence interval that includes zero. In both cases, more than 68% of data sets are consistent with a circular orbit at a 68% level using either method. Using the Γ analysis, $6.8 \pm 3.0\%$ more simulated data sets are consistent with a circular orbit than based on the standard MCMC analysis. This confirms our intuition that the Γ analysis is a less biased method for analyzing systems at very small eccentricity. Thus, the Γ analysis may be a useful tool in assessing the significance of a measurement of a small non-zero eccentricity. In particular, we find 5 cases (11.4%) in which $e_{lower} = 0$ for Γ analysis even though e_{lower} for MCMC is greater than zero (e.g., HD 46375, HD 76700, HD 7924, HD 168746, HD 102117).

A similar experiment is conducted except that an eccentricity of 0.2 is assigned to each system instead of zero eccentricity. Again, we assess the accuracy of the two methods by comparing the input and output eccentricities. When using the MCMC method, we find that the 68% credible interval for the eccentricity does not include the input eccentricity for $26.0 \pm 2.1\%$ of simulated data sets. When using the Γ method, we find that the 68% confidence interval for the eccentricity does not include the input eccentricity for $18.9 \pm 1.8\%$ of simulated data sets. Again, there is a larger fraction of results from the MCMC method that are not consistent with the input at a sizable eccentricity, indicating Γ analysis is less likely to reject the correct eccentricity. We also investigate the bias of the two methods at a significant eccentricity (i.e. $e=0.2$). In the cases where the output eccentricities are consistent with the input, we find that $47.9 \pm 3.3\%$ of the output eccentricities are below 0.2 while $52.1 \pm 3.5\%$ of outputs are over 0.2 for MCMC method indicating the MCMC method is not biased at a sizable eccentricity, which agrees with the finding from Zakamska et al. (2011). In comparison, Γ analysis is also an unbiased analysis with $49.9 \pm 3.3\%$ below input and $50.1 \pm 3.3\%$ exceeding input. Therefore, we find no evidence for significant bias of either method for data sets with a significant eccentricity.

3.3 Discussion of Γ Analysis

The different methods for analyzing Doppler observations are complementary. Bayesian methods and MCMC in particular are routinely used to sample from the posterior distribution for the Keplerian orbital parameters for a given system. However, the analysis of an exoplanet population is more complicated than simply

performing a Bayesian analysis of each system. To illustrate this point, consider a population of planets that all have exactly circular orbits. Due to measurement uncertainties and finite sampling, the “best-fit” eccentricity for each system will be non-zero. Similarly, since eccentricity is a positive-definite quantity, the analysis of each system will result in a posterior distribution that has significant support for $e > 0$. This property remains even if one combines many point estimates (e.g., “best-fit”), frequentist confidence intervals or Bayesian posterior distributions. While the posterior distribution for the orbital parameters represents the best possible analysis of an individual system, the inevitable bias for nearly circular orbits is a potential concern for population analyses. Therefore, it is important to apply different methods for population analyses (e.g., Hogg et al. (2010); Zakamska et al. (2011)).

Since we intend to investigate the potential role of tidal effects on the eccentricity distribution of short-period planets, we developed a hybrid technique to assess the sensitivity of our results to bias in the posterior distribution for planets with nearly circular orbits. This hybrid technique (Γ analysis) involves performing Bayesian analyses of each individual planetary system along with several simulated data sets, each of varying eccentricity. The MCMC analysis of each data set allows us to account for the varying precision of eccentricity measurements depending on the velocity amplitude, measurement precision, number of observations and phase coverage. We assess the extent of the eccentricity biases by performing the same analysis on simulated data sets with known eccentricity. We compare the posterior densities for the actual data set to the posterior density for each of the simulated data sets to determine which input model parameters are consistent with the observations. We can construct frequentist confidence intervals based on Monte Carlo simulations (i.e., comparing the posterior distributions for the synthetic data sets to each other).

The basic approach of the Γ analysis is similar to likelihood-free methods more commonly used in approximate Bayesian computation. In this case, we do have a likelihood which allows us to sample from the posterior probability distribution using standard MCMC. We compare the posterior densities calculated for several simulated data sets to the posterior density of the actual observations, so as to assess the accuracy and bias of the standard MCMC analysis.

The problem of biased eccentricity estimators for nearly circular orbits is familiar from previous studies of binary stars. In particular, Lucy & Sweeney (1971) investigated the possibility of mistakenly assigning an eccentric orbit to a circular spectroscopic binary due to inevitable measurement errors. As many spectroscopic binaries may have been affected by tidal circularization, they suggested assigning a circular orbit to any system for which the eccentricity credible interval contained 0. When studying a population of systems for which circular orbits are common, this approach significantly reduces the chance of erroneously concluding the system has a non-zero eccentricity. One obvious disadvantage of this approach is that it would lead to a negative bias for systems where the eccentricity is of order σ/K , where σ is the typical measurement precision and K is the velocity amplitude. For binary stars, σ/K may be small enough that this is not a significant concern. For exoplanets, where σ/K may be as small as $\sim 2 - 3$, such a procedure would result in a significant negative bias for many systems. The Γ analysis offers an alternative approach, which may be particularly useful when analyzing the eccentricity distribution of a population of planetary systems.

For the sake of comparison, we consider a modernized version of the Lucy & Sweeney (1971) approach which is based on

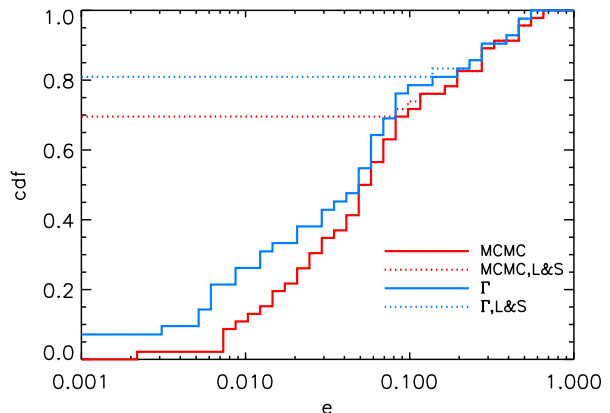


Figure 5. Cumulative distributions functions (CDFs) of eccentricities from different methods. The solid red line is for e_{MCMC} , adopted from MCMC method (Appendix A1). The dotted red line is similar to MCMC, but any eccentricity with e_{lower} of 0 for a 95% credible interval is assigned to 0. The blue lines are for Γ analysis, where the solid line is for e_{Γ} from the Γ analysis (Appendix A1) and the dotted line is similar, but any eccentricity with e_{lower} of 0 for a 95% confidence interval is assigned to 0.

the posterior distribution from a standard MCMC analysis or the confidence interval from our Γ analysis. We construct a histogram or cumulative distribution of the eccentricities for a population of systems, using a single summary statistic for each system: the posterior mean for the standard MCMC analysis or the eccentricity that maximizes the Γ statistic. Following Lucy & Sweeney (1971), we adopt an eccentricity of zero for any system for which the 95% significance level (Γ method) or the 95% credible interval (MCMC) includes $e = 0$. The cumulative distribution functions of the eccentricities using different methods are plotted in Fig. 5. Based on the generalized Lucy & Sweeney (1971) approach, $\sim 81\%$ (70%) of the short-period planet systems in our sample are consistent with circular orbits using the Γ analysis (standard MCMC analysis). Clearly, the Lucy & Sweeney (1971) approach results in a large fraction being assigned a circular orbit, largely due to the choice of a 95% threshold. The fraction assigned a circular orbit is sensitive to the size of the credible interval used when deciding whether to set each eccentricity to zero. There is no strong justification for the choice of the 95% threshold (as opposed to 68% or 99.9% threshold) and tuning the threshold to agree with other methods negates the primary advantage of the Lucy & Sweeney (1971) method, that it requires no additional computations. Therefore, we do not recommend using the Lucy & Sweeney (1971) approach to learn about the eccentricity distribution for a population when σ/K is not large.

4 TIDAL INTERACTION BETWEEN STAR AND PLANET

Several factors affect the eccentricity distribution of short-period planets including tidal interaction between host star and planet and possible perturbation of an undetected companion. We will discuss how these factors affect the eccentricity distribution and whether the effect is observable.

In order to understand the influence of tidal interaction on eccentricity distribution, we first divide our sample into two subsets, one subset contains systems with a long-term RV trend while the other subset contains systems that do not show a long-term RV trend (Fig. 6). The systems that are noted with a long-term ve-

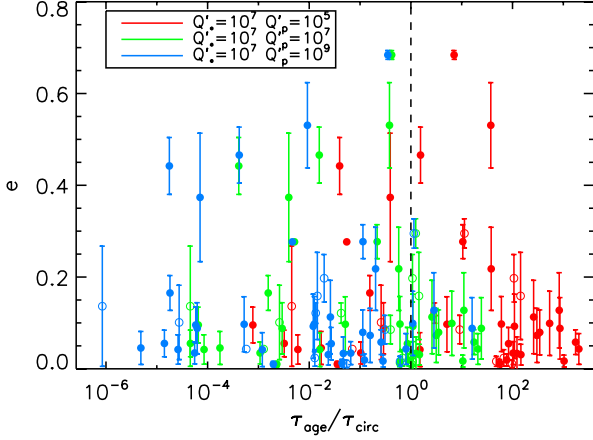


Figure 6. Distribution of short-period single-planet systems in $(e, \tau_{age}/\tau_{circ})$ space. Filled circles are systems showing no linear RV trend and open circles are systems showing long-term linear RV trends. Different colors indicate different combinations of Q'_* and Q'_p

locity trend include 51 PEG, BD -10 3166, GJ 436, GJ 86, HD 107148, HD 118203, HD 149143, HD 68988, HD 7924, HD 99492 and τ Boo. We further divide the no-trend subset into two groups, one group is distinguished by $\tau_{age}/\tau_{circ} \geq 1$, and the other group is distinguished by $\tau_{age}/\tau_{circ} < 1$, where τ_{circ} is tidal circularization time scale and τ_{age} is the age of the host star. We investigate whether there is a significant difference in the eccentricity distribution between these two groups as expected if tidal interaction is an important factor in shaping eccentricity distribution. Following Matsumura et al. (2008), we estimate τ_{circ} using:

$$\tau_{circ} = \frac{2}{81} \frac{Q'_p}{n} \frac{M_p}{M_*} \left(\frac{a}{R_p} \right)^5 \left[\frac{Q'_p}{Q'_*} \left(\frac{M_p}{M_*} \right)^2 \left(\frac{R_*}{R_p} \right)^5 F_* + F_p \right]^{-1}, \quad (5)$$

where the subscripts p and $*$ denote planet and star, M is mass, R is radius, a is semi-major axis, Q' is modified tidal quality factor and $n = [G(M_* + M_p)/a^3]^{1/2}$ is the mean motion. Matsumura et al. (2008) adopted 10^6 as a typical value for Q'_* for short period planetary system host stars and considered Q'_p ranging from 10^5 to 10^9 . We use $Q'_* = [10^6, 10^7]$ and $Q'_p = [10^5, 10^7, 10^9]$ in our analysis. The factors F_* and F_p are defined in the following two equations:

$$F_* = f_1(e^2) - \frac{11}{18} f_2(e^2) \frac{\Omega_{*,rot}}{n}, \quad (6)$$

$$F_p = f_1(e^2) - \frac{11}{18} f_2(e^2) \frac{\Omega_{p,rot}}{n}, \quad (7)$$

where Ω is rotational frequency. For short-period planets one could set $\Omega_{p,rot}/n = 1$ based on the assumption that all the planets in our sample have been synchronized since $\tau_{synch} \sim 10^{-3} \tau_{circ}$ (Rasio et al. 1996). In order to check whether our conclusion is sensitive to the choice of $\Omega_{*,rot}/n$, we conduct calculations with other $\Omega_{*,rot}/n$ values in which we choose stellar rotation period to be 3, 30, and 70 days for all the stars. We find that this range for $\Omega_{*,rot}/n$ does not change the conclusions in the paper. Therefore, for future discussion, we adopt $\Omega_{*,rot}/n = 0.67$, which results in stellar rotation periods consistent with typical values from 3 to 70 days (Matsumura et al. 2008). The uncertainties in $\Omega_{*,rot}/n$ are accounted for by our subsequent data analysis (Equation. 10). And f_1 and f_2 are approximated by the equations:

$$f_1(e^2) = \left(1 + \frac{15}{4} e^2 + \frac{15}{8} e^4 + \frac{5}{64} e^6 \right) / (1 - e^2)^{13/2}, \quad (8)$$

$$f_2(e^2) = \left(1 + \frac{3}{2} e^2 + \frac{1}{8} e^4 \right) / (1 - e^2)^5. \quad (9)$$

Planet radius R_p is estimated based on Fortney et al. (2007). We assume that the planet and host star are formed at the same epoch. We assume that planet structure is similar to Jupiter with a core mass fraction of $25M_{\oplus}/M_J = 7.86\%$. Radii of GJ 436 b and HD 149026 b are adopted from reference papers because there is a factor of >2 difference between observed values (Torres et al. 2008) and theoretically calculated values. Stellar radius and age estimations are obtained from the following sources with descending priority: 1, Takeda et al. (2007); 2, *nsted.ipac.caltech.edu*; 3, *exoplanet.eu*. The calculated τ_{circ} values are presented in Appendix A2 in addition to the results of MCMC analysis of individual system and other stellar and planetary properties.

We use the eccentricity posterior samples for each system for which the standard MCMC analysis was successful (i.e., results of §2.1) to construct the eccentricity samples of two groups separated by τ_{age}/τ_{circ} . We note that there are considerable uncertainties in the estimation of τ_{age} and τ_{circ} , so $\tau_{age}/\tau_{circ} > 1$ does not necessarily mean that the actual system age is larger than the actual circularization time. We consider the sensitivity of our results to these uncertainties by adopting a probability function:

$$\rho\left(\frac{\tau_{age}}{\tau_{circ}}\right) = \begin{cases} 1 - 0.5 \exp\left[-\eta \cdot \left(\frac{\tau_{age}}{\tau_{circ}} - 1\right)\right] & \text{if } \frac{\tau_{age}}{\tau_{circ}} \geq 1 \\ 0.5 \exp\left[-\eta \cdot \left(\frac{\tau_{circ}}{\tau_{age}} - 1\right)\right] & \text{if } \frac{\tau_{age}}{\tau_{circ}} < 1 \end{cases} \quad (10)$$

where η is a parameter tuning the confidence of τ_{age} and τ_{circ} estimation. For example, if $\tau_{age}/\tau_{circ} = 2$ and $\eta = 1$, then $\rho(\tau_{age}/\tau_{circ}) = 0.816$, meaning there is 81.6% chance that the system is from the group of $\tau_{age}/\tau_{circ} \geq 1$ because of the uncertainties in τ_{age} and τ_{circ} estimation. Therefore, we take 81.6% of the eccentricity posterior samples of the system to construct eccentricity sample for the group of $\tau_{age}/\tau_{circ} \geq 1$ and the remaining 18.4% eccentricity posterior samples to construct eccentricity sample for group of $\tau_{age}/\tau_{circ} < 1$. The η parameter reflects our confidence in τ_{age} and τ_{circ} estimation. If we are not very confident in the estimation of τ_{age} and τ_{circ} , then we set η to a small value approaching zero, so half of the eccentricity posterior samples for each system are assigned to the group with $\tau_{age}/\tau_{circ} \geq 1$ and the other half are assigned to the group with $\tau_{age}/\tau_{circ} < 1$. After constructing the eccentricity sample for the two groups, we use two-sample K-S test to test the null hypothesis that these two samples from two groups were drawn from the same parent distribution. The results (Table 1) show that we are unable to exclude the null hypothesis at a low p value (statistic of two-sample K-S test) because of the small effective sample size ($N' \sim 8$). If $\Delta_{max} = 0.2$, where Δ_{max} is the maximum difference between cumulative distribution functions of two groups, we can exclude the null hypothesis at $p = 0.05$ only if N' is more than 44. In comparison, our current sample size is inadequate to draw a statistically significant conclusion on whether or not the groups are from the same parent distribution. However, we do see a hint of a difference between cumulative distribution functions of two groups (Fig. 7 left), there are more systems with low-eccentricity for the group with $\tau_{age}/\tau_{circ} < 1$, which is a consequence of tidal circularization. We also find that the conclusion is unchanged for a wide range of η , Q'_* , and Q'_p values.

We conduct similar test for two subsets distinguished by whether or not a long-term velocity trend is recognized and find the similar result that our current sample size is inadequate to draw a statistically significant conclusion on whether or not the groups are from the same parent distribution. Again, we see a hint of a

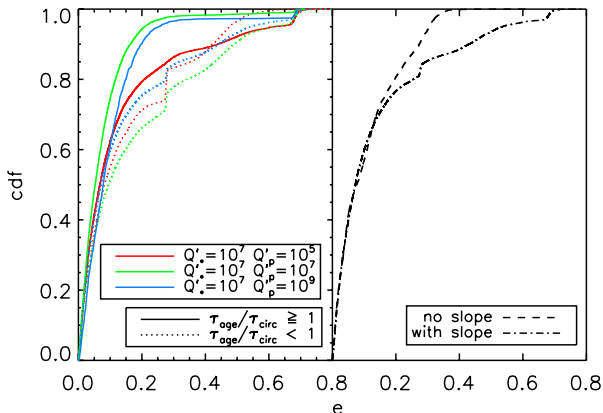


Figure 7. The left panel compares the cumulative distribution function of eccentricity for two groups of planets: 1) $\tau_{age}/\tau_{circ} \geq 1$ (solid line) and 2) $\tau_{age}/\tau_{circ} < 1$ (dotted line). The right panel compares cumulative distribution functions of eccentricity for two subsets of planets: planets without a long-term RV slope (dashed line) and planets with a long-term RV slope (dash-dotted line).

Table 1. Two-sample K-S test result. Δ_{max} is the maximum difference between cumulative distribution functions of eccentricity for two groups separated by $\tau_{age}/\tau_{circ} = 1$. N' is the effective sample size, calculated by $(N_1 \cdot N_2)/(N_1 + N_2)$, p is the significance level at which two-sample K-S test rejects the null hypothesis that the two eccentricity samples are from the same parent distribution; η is a parameter tuning the confidence of τ_{age} and τ_{circ} estimation.

		Q'_p	10^5	10^7	10^9
$Q'_* = 10^6$	$\eta=1000$	Δ_{max}	0.088	0.175	0.086
		N'	7.57	8.76	7.57
		p	1.00	0.93	1.00
	$\eta=1$	Δ_{max}	0.103	0.160	0.093
		N'	7.72	8.72	7.02
		p	1.00	0.97	1.00
	$\eta=0.001$	Δ_{max}	0.043	0.027	0.061
		N'	8.59	8.50	8.08
		p	1.00	1.00	1.00
$Q'_* = 10^7$	$\eta=1000$	Δ_{max}	0.088	0.286	0.190
		N'	7.57	8.42	2.80
		p	1.00	0.43	1.00
	$\eta=1$	Δ_{max}	0.103	0.259	0.168
		N'	7.72	8.36	2.81
		p	1.00	0.56	1.00
	$\eta=0.001$	Δ_{max}	0.040	0.027	0.065
		N'	8.61	8.39	7.67
		p	1.00	1.00	1.00

difference between cumulative distribution functions of two subsets (Fig. 7 right) although it is not statistically significant. There are more systems with low-eccentricity for subsets showing no sign of external perturbation. The maximum difference between the cumulative distribution functions Δ_{max} is 0.123, N' is 8.37 and K-S statistic is 0.999. In that case, we need an effective sample size of 119 in order to make a statistically significant conclusion ($p=0.05$). In other cases, larger sample size is required since Δ_{max} is less.

We have shown that any difference in eccentricity distribution depending on expected time scale for tidal circularization or the presence of additional bodies capable of exciting inner planet's eccentricity is not statistically significant, although this may be a consequence of small effective sample size. The data are also con-

sistent with the argument that both factors play roles in affecting the eccentricity distribution.

5 ECCENTRICITY DISTRIBUTION

We seek an analytical function that is able to approximate the observed eccentricity distribution for short period single planetary systems in the framework of Bayesian inference. For this purpose, we first exclude systems showing long-term RV trends to reduce the effect of perturbation on the estimated eccentricity distribution. We also assume that the distribution of τ_{age}/τ_{circ} in our sample is representative of short-period single-planet systems.

Using the posterior samples of eccentricity from standard MCMC analysis, we obtain an observed eccentricity probability density function (pdf) $f(e)$ by summing the posterior distributions together. While not statistically rigorous, this provides a simple summary of our results. Logarithmic binning is adopted because the shape of $f(e)$ at low eccentricity is of particular interest. The uncertainty $\sigma(e)$ for each bin is set by assuming a Poisson distribution. Then, we use a brute-force Bayesian analysis to find the most probable values of parameters for the candidate eccentricity pdf $f'(e)$ that approximates the observed eccentricity pdf. In the observed eccentricity pdf, there is a pile-up in small eccentricities near zero and a scatter of nonzero eccentricity less than 0.8. Therefore, we use a mixture of two distributions: an exponential pdf $f_{expo}(e, \lambda) = (1/\lambda) \cdot \exp(-e/\lambda)$ to represent the pile-up of small eccentricity near zero and either a uniform distribution or a Rayleigh distribution (Juric & Tremaine 2008) to represent the population with sizable eccentricities. We assume a uniform distribution for parameters in prior $\Sigma(\vec{\theta})$, where $\vec{\theta}$ is vector containing the parameters for $f'(e)$. Our results are not sensitive to the choice of priors. We adopt Poisson likelihood for each bin in the form of $f_{Poisson}(n; \nu) = (\nu^n \cdot \exp(-\nu))/n!$, i.e., $L(e_i|\vec{\theta}) = f_{Poisson}(f'(e_i|\vec{\theta}) \cdot N; f(e_i) \cdot N)$, where N is total number of posterior samples. The value of $f'(e_i|\vec{\theta}) \cdot N$ is rounded if it is not an integer. The posterior distribution of $\vec{\theta}$ is calculated as $p(\vec{\theta}|\vec{e}) = \left[\prod_i^M \Sigma(\vec{\theta}) L(e_i|\vec{\theta}) \right]^{1/M} / \int \left[\prod_i^M \Sigma(\vec{\theta}) L(e_i|\vec{\theta}) \right]^{1/M} d\vec{\theta}$, where M is the number of bins. We have explored a range of bin size from 10 to 40 bins in logarithmal space and conclude that the results of Bayesian analysis do not change significantly with choice of bin size. Since the plausible values of parameters for $f'(e)$ are limited, we do not have to explore a large parameter space. Therefore, a brute-force Bayesian analysis is practical.

We apply Bayesian analysis to three different planet populations for different η values ($\eta=0.001, 1, 1000$) assuming $Q'_* = 10^7$ and $Q'_p = 10^7$: 1) systems without a long-term RV slope and $\tau_{age}/\tau_{circ} \geq 1$; 2) systems without long-term RV slope and $\tau_{age}/\tau_{circ} < 1$; 3) the union of 1) and 2). The results of Bayesian analysis are presented in Table 2. Fig 8 shows marginalized probability density of different parameters for analytical eccentricity distribution with a mixture of exponential and Rayleigh distributions ($f'(e) = \alpha \cdot f_{expo}(e, \lambda) + (1 - \alpha) \cdot f_{rayl}(e, \sigma)$). α is the fraction of exponential distribution component and $f_{rayl}(e, \sigma)$ represents Rayleigh distribution with the form of $f_{rayl}(e, \sigma) = (e/\sigma^2) \cdot \exp(-e^2/2\sigma^2)$. Group 1 (potentially circularized system) is represented by dashed lines of different colors indicating different values of η while group 2 (systems unlikely to have been circularized) is represented by colored solid lines. Group 1 and group 2 are well mixed if $\eta=0.001$, i.e., a loose constraint is applied on the boundary of $\tau_{age}/\tau_{circ} = 1$.

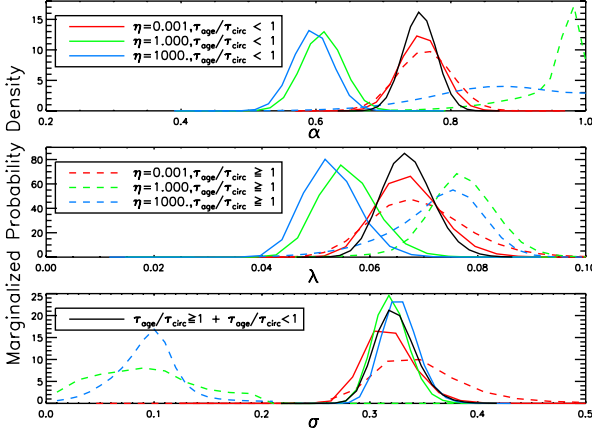


Figure 8. Marginalized probability density functions of parameters for analytical eccentricity distribution with a mixture of exponential and Rayleigh pdfs. Uncircularized systems (group 2) are represented by colored solid lines while circularized systems (group 1) are represented by colored dashed lines. Different colors indicate different η values, red: $\eta = 0.001$; green: $\eta = 1$; blue: $\eta = 1000$. Solid black lines are for union of group 1 and 2.

When adopting $\eta=0.001$, the marginalized posterior pdfs for both groups 1 and 2 approach the marginalized pdf for group 3 (solid black lines; the union of group 1 and 2, including all planets without a velocity slope). When we adopt larger η values ($\eta=1$ or 1000), α , the fraction of the exponential component of the pdf is greater for group 1 (Fig 8 top: blue and green dashed lines) than group 2 (Fig 8 top: blue and green solid lines). This is consistent with the hypothesis that significant tidal circularization affected group 1. For group 1, the fraction of the exponential component of the pdf is consistent with unity, implying that the eccentricity distribution for planets from group 1 can be described by an exponential pdf. In comparison, there is a substantial fraction of Rayleigh component (40%) for the analytical function describing eccentricity distribution for uncircularized systems (i.e., group 2). Similar conclusions are also drawn for the analytical eccentricity distribution with a mixture of exponential and uniform distribution (Fig 9) in the form of $f'(e) = \alpha \cdot f_{\text{expo}}(e, \lambda) + (1 - \alpha) \cdot f_{\text{unif}}(e, \beta)$, where $f_{\text{unif}}(e, \beta)$ is uniform distribution with lower boundary of 0 and upper boundary of β . Fig. 10 shows the cumulative distribution of the eccentricities sample based on summing the posterior eccentricity samples of each system (green solid line) and the CDFs of the two analytic functions (blue dotted and dashed) with the parameters that maximize the posterior probability (see Table 2, subset 3). For comparison, the cumulative distribution of e_{MCMC} from standard MCMC analysis (Appendix A1) is shown in red. The difference between the red and the green line cannot be distinguished at 0.05 significant level in a K-S test ($N'=46$).

In order to check whether the analytical function with the most probable parameters is an acceptable approximation to the eccentricity distribution for short-period single-planet systems, we generate test samples from the analytical functions and compare the resulting eccentricity samples to observations. For each test sample there are N' eccentricities following the distribution of the analytical function $f'(e|\hat{\theta})$, where N' is the effective sample size. Each eccentricity is perturbed by a simulated measurement error that follows the distribution of posterior samples for our analysis of the actual observations. The test sample is then compared to the observed eccentricity samples obtained by standard MCMC analysis using

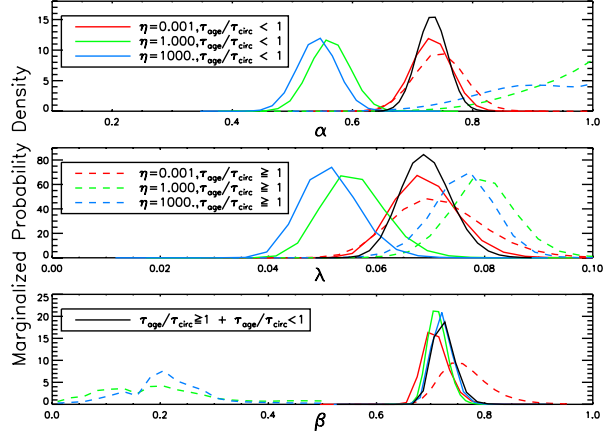


Figure 9. Marginalized probability density functions of parameters for analytical eccentricity distribution with a mixture of exponential and uniform pdf. Uncircularized systems (group 2) are represented by colored solid lines while circularized systems (group 1) are represented by colored dashed lines, red: $\eta = 0.001$; green: $\eta = 1$; blue: $\eta = 1000$. Different colors indicate different η values. Solid black lines are for union of group 1 and 2.

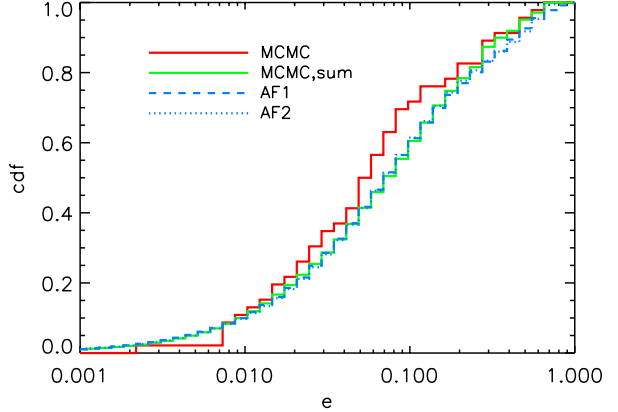


Figure 10. Cumulative distributions functions (cdf) of eccentricities from different methods. MCMC: most probable eccentricities, e_{MCMC} , adopted from MCMC method (Appendix A1); MCMC, sum: eccentricities by summing up posterior distribution samples of each system; AF1: cdf of the analytical function with the most probable parameters, $f'(e) = \alpha \cdot f_{\text{expo}}(e, \lambda) + (1 - \alpha) \cdot f_{\text{rayl}}(e, \sigma)$; AF2: cdf of the analytical function with the most probable parameters, $f'(e) = \alpha \cdot f_{\text{expo}}(e, \lambda) + (1 - \alpha) \cdot f_{\text{unif}}(e, \beta)$.

two-sample K-S test. We report in Table 2 the percentage of trials in which eccentricity samples generated by our analytical function can not be differentiated from the observed eccentricity sample at 0.05 confidence level. All the candidate analytical functions we have tested are able to reproduce the observed eccentricity distribution in more than 99.6% of the trials at 0.05 confidence level. We conclude that the best-fit analytical function is an adequate approximation to observed eccentricity distribution. We also compare to analytical eccentricity distribution used in Shen & Turner (2008) $f'(e) \sim [1/(1+e)^4 - e/2^2]$ in which $a=4$, although it is not specifically for short period single planetary systems. Similar to what we did in previous test, we found that in 39.0% of the tests, the eccentricity samples generated by analytical functions can not be differentiated from the observed eccentricity sample at 0.05 confidence level.

Table 2. Bayesian analysis results. Group 1: systems without long-term RV slope and $\tau_{age}/\tau_{circ} \geq 1$; group 2: systems without long-term RV slope and $\tau_{age}/\tau_{circ} < 1$; group 3: union of 1 and 2. Numbers in bracket are uncertainties of the last two digits. The *fraction* column reports the percentage of trials in which eccentricity testing samples generated by analytical function can not be differentiated from the observed eccentricity sample at 0.05 confidence level.

η	subset	$f'(e) = \alpha \cdot f_{expo}(e, \lambda) + (1 - \alpha) \cdot f_{grav}(e, \sigma)$				$f'(e) = \alpha \cdot f_{expo}(e, \lambda) + (1 - \alpha) \cdot f_{unif}(e, \beta)$			
		$\lambda[\times 10^{-2}]$	$\alpha[\times 10^{-1}]$	$\sigma[\times 10^{-1}]$	fraction	$\lambda[\times 10^{-2}]$	$\alpha[\times 10^{-1}]$	$\beta[\times 10^{-1}]$	fraction
0.001	1	6.83(84)	7.61(40)	3.38(36)	100.0%	7.08(82)	7.35(38)	7.56(41)	100.0%
	2	6.67(59)	7.56(32)	3.15(22)	100.0%	6.86(59)	7.32(33)	7.06(23)	100.0%
1.000	1	7.71(58)	9.78(20)	0.83(54)	99.6%	7.96(59)	10.0(12)	1.8(11)	99.9%
	2	5.55(53)	6.10(31)	3.19(16)	100.0%	5.55(57)	5.66(34)	7.12(18)	100.0%
1000.	1	7.41(72)	8.9(12)	0.95(24)	99.9%	7.62(56)	9.2(11)	2.10(57)	100.0%
	2	5.24(49)	5.95(30)	3.27(16)	100.0%	5.11(53)	5.44(33)	7.20(19)	100.0%
	3	6.67(47)	7.54(25)	3.22(19)	100.0%	6.89(47)	7.33(26)	7.22(20)	100.0%

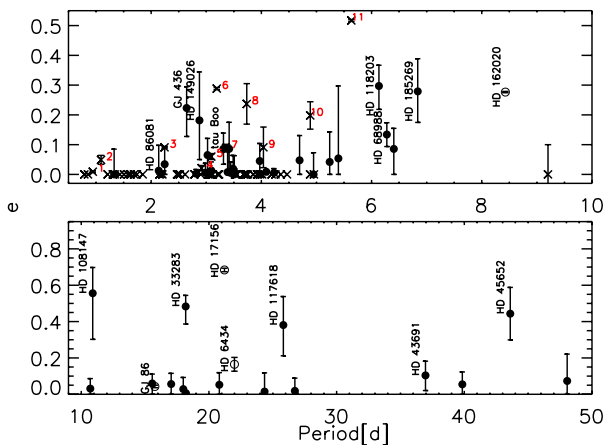


Figure 11. Distribution of short-period single-planet systems in our sample in period-eccentricity space (top: $p \leq 10$ day; bottom: $p > 10$ day). Systems that are not consistent with zero eccentricity according to Γ analysis (filled circles) or MCMC analysis (open circles) are marked with corresponding names. We also include transiting planets (marked as cross) for comparison. Transiting systems not consistent with zero eccentricity are marked with numbers: 1, WASP-18; 2, WASP-12; 3, WASP-14; 4, HAT-P-13; 5, WASP-10; 6, XO-3; 7, WASP-6; 8, WASP-17; 9, CoRoT-5; 10, HAT-P-11; 11, HAT-P-2.

From the results of Bayesian analysis, there is a clear difference in α , the fraction of exponential distribution, between group 1 and 2, suggesting the role played by tidal circularization. Group 1 with $\tau_{age}/\tau_{circ} \geq 1$ shows more planets with near-zero eccentricities ($\alpha \sim 75\%$) as compared to group 2 ($\alpha \sim 55\%$) with $\tau_{age}/\tau_{circ} < 1$ (Table 2). Since the eccentricity samples tested were perturbed by measurement errors, the analytical function we found can be interpreted as an approximation of the underlying eccentricity distribution of short-period single-planet systems. However, the actual parameter values and uncertainties in the analytical function are dependent upon the quality of observation and the number of systems in the sample of short-period single planets. As the measurement precision and the sample size improve, we will be able to better constrain the values of parameters in the analytical function which approximates the underlying eccentricity distribution.

6 DISCUSSION

The median eccentricity of short-period single-planet systems in our sample is 0.088. When compared to median eccentricity for all the detected exoplanets 0.15, it suggests that the population may be affected by tidal circularization. We use eccentricity estimated

by Γ analysis in the following discussion since it is a less biased method for accessing small eccentricity. Fig. 11 shows the period-eccentricity correlation. We would expect planets with sufficient short period to be tidally circularized. While this is generally true, there are 3 (17.6%) planets with $P < 4d$ and non-circular orbits: GJ 436, HD 149026 and τ Boo. For GJ 436, it is suspected that an outer companion may be pumping the eccentricity (Maness et al. 2007; Ribas et al. 2008). Similarly, observations of τ Boo b are inconsistent with circular orbit, but might be explained by the perturbation of an unseen companion indicated by a long-term RV linear trend (Butler et al. 2006). Secondary eclipse timing indicates that the eccentricity of HD 149026 is quite small but inconsistent with zero (Knutson et al. 2009). Considering planets with orbital periods up to 10 days, there are 4 additional systems that are not circularized. HD 118203, HD 68988 and HD 185269 might be due to perturbations by additional bodies in the system (Butler et al. 2006) while the non-zero eccentricity of HD 162020 b may be attributed to a different formation mechanism (Udry et al. 2002). With period longer than 10 days, there are 8 (44.4%) planets with $\tau_{age}/\tau_{circ} > 1$ which have non-zero eccentricity and no detected long-term linear trend. In comparison, there are 8 (28.6%) eccentric planets with orbital periods less than 10 days. The increasing fraction of recognizably eccentric orbits as period increases is suggestive of decreasing tidal circularization effect, but large sample of planets is required to draw firm conclusion. The discovery of over 705 planets candidates by the Kepler mission presents an excellent opportunity to analyze the eccentricity distribution of short-period planets (Ford et al. 2008; Borucki et al. 2011). We briefly consider transiting planets. We note that 11 of 58 (19.0%) transiting systems as of June 2010 are not consistent with zero eccentricity, and the orbital periods for all transiting planets but 3 (i.e. CoRoT-9b, HAT-P-13c HD 80606b) are less than 10 days. We infer that the tidal circularization process might be effective for isolated planets with orbital period of less than 10 days. Alternatively, the planet formation and migration processes for short-period giant planet may naturally lead to a significant fraction of nearly circular orbits, even before tidal effect takes place.

It is worth noting that HD 17156 b (Fischer et al. 2007) has one of the most eccentric orbits among short-period planet systems in spite the fact that τ_{age}/τ_{circ} could be well over 10 (Fig 6, red). However, Barbieri et al. (2009) found no indications of additional companions based on observations of directing imaging, RV and astrometry measurement. Anglada-Escudé et al. (2010) investigated the possibility that a 2:1 resonant orbit can be hidden by an eccentric orbital solution. It is interesting to explore such possibility on this particular system to solve the discrepancy of high eccentricity and τ_{age} to τ_{circ} ratio. Another possibility is that the system is in the process of circularization that began well after the

star and planet formed (e.g., due to planets scattering). However, we are cautious in drawing conclusions since τ_{age}/τ_{circ} could be less than unity (Fig 6, green and blue).

7 CONCLUSION

We apply standard MCMC analysis for 50 short-period single-planet systems and construct a catalog of orbital solutions for these planetary systems (Appendix A2). We find general agreement between MCMC analysis and previous references with the primary exception being cases where eccentricity was held fixed in previous analysis. We develop a new method to test the significance of non-circular orbits (Γ analysis), which is better suited to performing population analysis. We find the eccentricity estimations from Γ analysis are consistent with results from both standard MCMC analysis and previous references.

Our results suggest that both tidal interactions and external perturbations may play roles in shaping the eccentricity distribution of short-period single-planet systems but large sample sizes are needed to provide sufficient sensitivity to make these trends statistically significant. We identify two analytical functions that approximate the underlying eccentricity distribution: 1) mixture of an exponential distribution and a uniform distribution and 2) a mixture of an exponential distribution and a Rayleigh distribution. We use Bayesian analysis to find the most probable values of parameters for the analytical functions given the observed eccentricities (Table 2). The analytical functions can be interpreted as the underlying distribution of eccentricities for short-period single-planet systems. Thus, the analytical functions can be used in the future theoretical works or as priors for eccentricity distribution.

ACKNOWLEDGMENTS

We thank Matthew Payne, Margaret Pan and Nadia Zakamska for useful discussions. This research was partially supported by NASA Origins of Solar Systems grant NNX09AB35G. This material is based upon work supported by the National Science Foundation under Grant No. 0707203.

REFERENCES

- Anglada-Escudé G., López-Morales M., Chambers J. E., 2010, *ApJ*, 709, 168
- Barbieri M., Alonso R., Desidera S., Sozzetti A., Martinez Fiorenzano A. F., Almenara J. M., Ceconi M., Claudi R. U., Charbonneau D., Endl M., Granata V., Gratton R., Laughlin G., Loeillet B., Amateur Consortium E., 2009, *A&A*, 503, 601
- Bonfils X., Mayor M., Delfosse X., Forveille T., Gillon M., Perrier C., Udry S., Bouchy F., Lovis C., Pepe F., Queloz D., Santos N. C., Bertaux J., 2007, *A&A*, 474, 293
- Borucki W. J., Koch D. G., Basri G., Batalha N., Boss A., Brown T. M., Caldwell D., Christensen-Dalsgaard J., Cochran W. D., DeVore E., Dunham E. W., Dupree A. K., Gautier III T. N., Geary J. C., Gilliland R., 2011, *ApJ*, 728, 117
- Bouchy F., Udry S., Mayor M., Moutou C., Pont F., Iribarne N., da Silva R., Illovaisky S., Queloz D., Santos N. C., Ségransan D., Zucker S., 2005, *A&A*, 444, L15
- Butler R. P., Wright J. T., Marcy G. W., Fischer D. A., Vogt S. S., Tinney C. G., Jones H. R. A., Carter B. D., Johnson J. A., McCarthy C., Penny A. J., 2006, *ApJ*, 646, 505
- Charbonneau D., 2003, in D. Deming & S. Seager ed., *Scientific Frontiers in Research on Extrasolar Planets Vol. 294 of Astronomical Society of the Pacific Conference Series*, HD 209458 and the Power of the Dark Side. pp 449–456
- da Silva R., Udry S., Bouchy F., Mayor M., Moutou C., Pont F., Queloz D., Santos N. C., Ségransan D., Zucker S., 2006, *A&A*, 446, 717
- da Silva R., Udry S., Bouchy F., Moutou C., Mayor M., Beuzit J., Bonfils X., Delfosse X., Desort M., Forveille T., Galland F., Hébrard G., Lagrange A., Loeillet B., Lovis C., Pepe F., 2007, *A&A*, 473, 323
- Fischer D. A., Laughlin G., Marcy G. W., Butler R. P., Vogt S. S., Johnson J. A., Henry G. W., McCarthy C., Ammons M., Robinson S., Strader J., Valenti J. A., 2006, *ApJ*, 637, 1094
- Fischer D. A., Vogt S. S., Marcy G. W., Butler R. P., Sato B., Henry G. W., Robinson S., Laughlin G., Ida S., Toyota E., Omiya M., Driscoll P., Takeda G., Wright J. T., Johnson J. A., 2007, *ApJ*, 669, 1336
- Ford E. B., 2006, *ApJ*, 642, 505
- Ford E. B., Gregory P. C., 2007, in G. J. Babu & E. D. Feigelson ed., *Statistical Challenges in Modern Astronomy IV Vol. 371 of Astronomical Society of the Pacific Conference Series*, Bayesian Model Selection and Extrasolar Planet Detection. pp 189–+
- Ford E. B., Quinn S. N., Veras D., 2008, *ApJ*, 678, 1407
- Ford E. B., Rasio F. A., 2008, *ApJ*, 686, 621
- Fortney J. J., Marley M. S., Barnes J. W., 2007, *ApJ*, 659, 1661
- Forveille T., Bonfils X., Delfosse X., Gillon M., Udry S., Bouchy F., Lovis C., Mayor M., Pepe F., Perrier C., Queloz D., Santos N., Bertaux J., 2009, *A&A*, 493, 645
- Gaudi B. S., Seager S., Mallen-Ornelas G., 2005, *ApJ*, 623, 472
- Ge J., van Eyken J., Mahadevan S., DeWitt C., Kane S. R., Cohen R., Vanden Heuvel A., Fleming S. W., Guo P., Henry G. W., Schneider D. P., Ramsey L. W., Wittenmyer R. A., Endl M., Cochran W. D., Ford E. B., Martín E. L., Israelian G., 2006, *ApJ*, 648, 683
- Gregory P. C., 2005, *ApJ*, 631, 1198
- Hogg D. W., Myers A. D., Bovy J., 2010, *ApJ*, 725, 2166
- Howard A. W., Johnson J. A., Marcy G. W., Fischer D. A., Wright J. T., Henry G. W., Giguere M. J., Isaacson H., Valenti J. A., Anderson J., Piskunov N. E., 2009, *ApJ*, 696, 75
- Johnson J. A., Marcy G. W., Fischer D. A., Laughlin G., Butler R. P., Henry G. W., Valenti J. A., Ford E. B., Vogt S. S., Wright J. T., 2006, *ApJ*, 647, 600
- Jurić M., Tremaine S., 2008, *ApJ*, 686, 603
- Knutson H. A., Charbonneau D., Cowan N. B., Fortney J. J., Showman A. P., Agol E., Henry G. W., 2009, *ApJ*, 703, 769
- Lo Curto G., Mayor M., Clausen J. V., Benz W., Bouchy F., Lovis C., Moutou C., Naef D., Pepe F., Queloz D., Santos N. C., Sivan J., Udry S., Bonfils X., Delfosse X., Mordasini C., Fouqué P., Olsen E. H., Pritchard J. D., 2006, *A&A*, 451, 345
- Lucy L. B., Sweeney M. A., 1971, *ApJ*, 76, 544
- Maness H. L., Marcy G. W., Ford E. B., Hauschildt P. H., Shreve A. T., Basri G. B., Butler R. P., Vogt S. S., 2007, *PASP*, 119, 90
- Marcy G. W., Butler R. P., 1996, *ApJ*, 464, L147+
- Marcy G. W., Butler R. P., Vogt S. S., Fischer D. A., Henry G. W., Laughlin G., Wright J. T., Johnson J. A., 2005, *ApJ*, 619, 570
- Matsumura S., Takeda G., Rasio F. A., 2008, *ApJ*, 686, L29
- Mayor M., Queloz D., 1995, *Nature*, 378, 355
- Mayor M., Udry S., Naef D., Pepe F., Queloz D., Santos N. C., Burnet M., 2004, *A&A*, 415, 391
- Melo C., Santos N. C., Gieren W., Pietrzynski G., Ruiz M. T., Sousa S. G., Bouchy F., Lovis C., Mayor M., Pepe F., Queloz

- D., da Silva R., Udry S., 2007, *A&A*, 467, 721
- Moutou C., Mayor M., Bouchy F., Lovis C., Pepe F., Queloz D., Santos N. C., Udry S., Benz W., Lo Curto G., Naef D., Ségransan D., Sivan J., 2005, *A&A*, 439, 367
- Pepe F., Mayor M., Queloz D., Benz W., Bonfils X., Bouchy F., Lo Curto G., Lovis C., Mégevand D., Moutou C., Naef D., Rupprecht G., Santos N. C., Sivan J., Sosnowska D., Udry S., 2004, *A&A*, 423, 385
- Rasio F. A., Tout C. A., Lubow S. H., Livio M., 1996, *ApJ*, 470, 1187
- Ribas I., Font-Ribera A., Beaulieu J., 2008, *ApJ*, 677, L59
- Santos N. C., Udry S., Bouchy F., da Silva R., Loeillet B., Mayor M., Moutou C., Pont F., Queloz D., Zucker S., Naef D., Pepe F., Sgransan D., Boisse I., Bonfils X., Delfosse X., Desert M., 2008, *A&A*, 487, 369
- Sato B., Fischer D. A., Henry G. W., Laughlin G., Butler R. P., Marcy G. W., Vogt S. S., Bodenheimer P., Ida S., Toyota E., Wolf A., Valenti J. A., Boyd L. J., Johnson J. A., Wright J. T., Ammons M., 2005, *ApJ*, 633, 465
- Shen Y., Turner E. L., 2008, *ApJ*, 685, 553
- Takeda G., Ford E. B., Sills A., Rasio F. A., Fischer D. A., Valenti J. A., 2007, *ApJs*, 168, 297
- Takeda G., Rasio F. A., 2005, *ApJ*, 627, 1001
- Torres G., Winn J. N., Holman M. J., 2008, *ApJ*, 677, 1324
- Udry S., Mayor M., Benz W., Bertaux J., Bouchy F., Lovis C., Mordasini C., Pepe F., Queloz D., Sivan J., 2006, *A&A*, 447, 361
- Udry S., Mayor M., Naef D., Pepe F., Queloz D., Santos N. C., Burnet M., 2002, *A&A*, 390, 267
- Winn J. N., Holman M. J., Henry G. W., Torres G., Fischer D., Johnson J. A., Marcy G. W., Shporer A., Mazeh T., 2009, *ApJ*, 693, 794
- Winn J. N., Johnson J. A., Marcy G. W., Butler R. P., Vogt S. S., Henry G. W., Roussanova A., Holman M. J., Enya K., Narita N., Suto Y., Turner E. L., 2006, *ApJL*, 653, L69
- Wolszczan A., 1994, *Science*, 264, 538
- Wright J. T., Butler R. P., Marcy G. W., Vogt S. S., Fischer D. A., Tinney C. G., Jones H. R. A., 2005, in *Bulletin of the American Astronomical Society Vol. 37 of Bulletin of the American Astronomical Society, Properties of the Known Nearby Exoplanets*. p. 1269
- Zakamska N. L., Pan M., Ford E. B., 2011, *MNRAS*, 410, 1895
- Zhou J., Lin D. N. C., 2007, *ApJ*, 666, 447
- Zucker S., Mazeh T., Santos N. C., Udry S., Mayor M., 2004, *A&A*, 426, 695

APPENDIX A:

A1 Comparison of Eccentricities Calculated From Different Methods

Name	Ref.		MCMC			Γ		
	e_{ref}	δe_{ref}	e_{MCMC}	e_{lower}	e_{upper}	e_{Γ}	e_{lower}	e_{upper}
HD 41004 B	0.081	0.012	0.058	0.000	0.109	0.000	0.000	0.085
HD 86081	0.008	0.004	0.058	0.008	0.166	0.013	0.001	0.098
HD 189733	0.000	0.000
HD 212301	0.000	...	0.015	0.000	0.051	0.034	0.000	0.091
GJ 436	0.159	0.052	0.191	0.146	0.248	0.223	0.128	0.295
HD 63454	0.000	...	0.018	0.000	0.038	0.003	0.000	0.017
HD 149026	0.000	...	0.192	0.118	0.270	0.182	0.050	0.344
HD 83443	0.012	0.023	0.007	0.000	0.020	0.006	0.000	0.037
HD 46375	0.063	0.026	0.052	0.030	0.084	0.065	0.000	0.121
HD 179949	0.022	0.015	0.014	0.000	0.024	0.013	0.000	0.042
τ Boo	0.023	0.015	0.079	0.054	0.117	0.086	0.034	0.139
HD 330075	0.000	...	0.019	0.000	0.087	0.008	0.000	0.095
HD 88133	0.133	0.072	0.076	0.000	0.127	0.086	0.000	0.175
HD 2638	0.000	...	0.041	0.000	0.076	0.005	0.000	0.042
BD -10 3166	0.019	0.023	0.010	0.000	0.030	0.019	0.000	0.064
HD 75289	0.034	0.029	0.021	0.000	0.043	0.000	0.000	0.063
HD 209458	0.000	...	0.008	0.000	0.016	0.005	0.000	0.018
HD 219828 ¹	0.000
HD 76700	0.095	0.075	0.062	0.003	0.104	0.045	0.000	0.104
HD 149143	0.000	...	0.012	0.000	0.022	0.009	0.000	0.014
HD 102195	0.000
51 Peg	0.013	0.012	0.007	0.000	0.014	0.006	0.000	0.020
GJ 674 ²	0.100	0.020	0.070	0.000	0.147	0.047	0.000	0.131
HD 49674	0.087	0.095	0.050	0.000	0.119	0.000	0.000	0.073
HD 109749	0.000	...	0.045	0.000	0.070	0.042	0.000	0.143
HD 7924	0.170	0.160	0.119	0.022	0.224	0.054	0.000	0.297
HD 118203	0.309	0.014	0.293	0.264	0.328	0.297	0.218	0.367
HD 68988	0.125	0.009	0.118	0.096	0.143	0.134	0.094	0.174
HD 168746	0.107	0.080	0.079	0.025	0.139	0.086	0.000	0.155
HD 185269 ³	0.276	0.037	0.276	0.242	0.314	0.279	0.175	0.389
HD 162020	0.277	0.002	0.277	0.274	0.279
GJ 176 ⁴	0.000
HD 130322	0.011	0.020	0.007	0.000	0.052	0.031	0.000	0.086
HD 108147	0.530	0.120	0.526	0.429	0.624	0.556	0.302	0.698
HD 4308	0.000	0.010	0.068	0.000	0.123	0.060	0.000	0.111
GJ 86	0.042	0.007	0.042	0.034	0.051
HD 99492	0.050	0.120	0.036	0.000	0.125	0.056	0.000	0.115
HD 27894	0.049	0.008	0.024	0.000	0.045	0.029	0.000	0.093
HD 33283	0.480	0.050	0.458	0.401	0.523	0.483	0.386	0.544
HD 195019	0.014	0.004	0.002	0.000	0.007	0.006	0.000	0.014
HD 102117	0.121	0.082	0.068	0.038	0.121	0.052	0.000	0.119
HD 17156 ⁵	0.684	0.013	0.683	0.672	0.691
HD 6434	0.170	0.030	0.159	0.124	0.202
HD 192263	0.055	0.039	0.026	0.000	0.055	0.015	0.000	0.118
HD 117618	0.420	0.170	0.352	0.233	0.511	0.381	0.212	0.538
HD 224693	0.050	0.030	0.031	0.000	0.055	0.019	0.000	0.089
HD 43691 ⁶	0.140	0.020	0.090	0.055	0.133	0.104	0.021	0.182
ρ Crb	0.057	0.028	0.048	0.000	0.069	0.055	0.000	0.123
HD 45652 ⁷	0.380	0.060	0.434	0.371	0.496	0.443	0.299	0.588
HD 107148	0.050	0.170	0.028	0.000	0.141	0.073	0.000	0.221

References: 1 Melo et al. (2007); 2 Bonfils et al. (2007); 3 Johnson et al. (2006); 4 Forveille et al. (2009); 5 Barbieri et al. (2009); 6 da Silva et al. (2007); 7 Santos et al. (2008); e_{ref} and δe_{ref} are from Butler et al. (2006) if otherwise noted.

A2 Catalog of Short-Period Single-Planet Systems

Name	P (day)	K ($m \cdot s^{-1}$)	e	ω (deg)	$M0$ (deg)	τ (day)	trend ($m \cdot s^{-1} \cdot d^{-1}$)	Jitter ($m \cdot s^{-1}$)	N_{obs}	M_* (M_{\odot})	R_* (R_{\odot})	M_P (M_J)	R_P (R_J)	τ_{circ} (Gyr)	τ_{age} (Gyr)	RV ref.
HD 41004B	1.32363±8.91594e-05	4599.21±337.57	0.0580 ^{+0.0511} _{-0.0580}	149.0±72.2	119.5±72.1	2452532.699	...	2761.45±168.90	149	0.40	0.40	18.40	1.06	0.26	6.32	7
HD 86081	1.99809±0.00677822	189.65±12.09	0.0575 ^{+0.01080} _{-0.0501}	-27.4±71.5	64.8±74.5	2453753.2	...	32.13±5.74	26	1.21	1.22	1.50	1.08	0.56	6.21	8
HD 189733 ¹	2.2186±0.0005	205±6	0±0.0002	90	270	2454037.612	...	15	86	9
HD 212301	2.24571±0.000147699	57.26±3.01	0.0147 ^{+0.0365} _{-0.0147}	172.8±85.6	56.0±85.6	2453388.9	...	8.53±1.78	23	1.05	1.19	0.40	1.07	0.28	5.90	11
GJ 436	2.64394±9.85041e-05	18.07±1.03	0.1912 ^{+0.0578} _{-0.0449}	-5.6±15.3	-66.6±14.5	2452992.1	0.0037±0.001 ⁵	0.41±1.46	55	0.41	0.46	0.07	0.38	5.57	6.00	6
HD 63454	2.81747±0.000382247	63.19±1.82	0.0177 ^{+0.0203} _{-0.0177}	-122.9±76.2	25.7±76.3	2453238.057	...	5.70±1.22	26	0.80	0.78	0.39	1.06	0.67	1.00	12
HD 149026	2.87807±0.00146571	54.63±11.90	0.1918 ^{+0.0743} _{-0.0155}	114.2±25.9	10.9±22.5	2453545.35	...	2.41±3.26	17	1.30	1.50	0.36	0.65	3.46	2.00	6
HD 83443	2.98572±5.30373e-05	56.00±1.05	0.0070 ^{+0.0320} _{-0.0070}	117.3±82.2	134.0±82.0	2452248.9	...	3.12±1.67	51	1.00	1.02	0.40	1.04	1.10	11.68	6
HD 46375	3.02358±6.44902e-05	33.67±0.81	0.0524 ^{+0.0229} _{-0.0229}	113.7±34.3	-53.2±34.3	2451920.7	...	3.28±0.60	50	0.92	0.94	0.23	1.02	0.67	11.88	6
HD 179949	3.0925±3.30046e-05	112.62±1.77	0.0104 ^{+0.0099} _{-0.0104}	-170.7±63.4	42.4±63.3	2452419.1	...	9.44±1.06	88	1.21	1.22	0.92	1.05	2.90	2.56	6
τ Boo	3.31249±3.12595e-05	469.59±14.86	0.0787 ^{+0.0382} _{-0.0246}	-141.6±25.0	24.4±24.9	2450529.2	-0.051±0.003 ⁶	94.30±8.13	98	1.35	1.33	4.13	1.06	4.12	1.64	6
HD 88133	3.41566±0.000841134	34.13±3.57	0.0761 ^{+0.0508} _{-0.0761}	-2.8±60.4	-39.5±60.1	2453180.0	...	5.67±1.61	21	1.20	1.93	0.30	1.00	1.49	9.56	6
HD 2638	3.43752±0.00823876	66.26±2.83	0.0407 ^{+0.0351} _{-0.0407}	126.9±78.6	-123.4±77.7	2453323.282	...	5.48±4.87	28	0.93	1.01	0.48	1.04	2.38	3.00	12
BD -10 3166	3.4878±0.000104858	60.53±1.44	0.0104 ^{+0.0192} _{-0.0104}	-14.6±83.9	36.6±83.7	2451844.7	0.005±0.002 ⁶	4.00±1.74	31	1.01	0.84	0.46	1.03	2.70	1.84	6
HD 75289	3.50928±7.2946e-05	54.84±1.87	0.0211 ^{+0.0211} _{-0.0211}	136.3±73.9	-162.2±74.1	2452593.9	...	4.73±1.73	30	1.21	1.28	0.47	1.03	3.03	3.28	6
HD 209458	3.52472±2.81699e-05	84.30±0.88	0.0082 ^{+0.0078} _{-0.0082}	43.8±68.4	92.5±68.5	2452499.3	...	3.27±0.86	64	1.14	1.14	0.69	1.05	4.07	2.44	6
HD 330075	3.6413±0.00187111	97.84±8.79	0.0187 ^{+0.0684} _{-0.0187}	38.2±91.6	35.2±91.7	2452968.399	...	24.59±5.00	21	0.70	0.90	0.62	1.06	1.97	6.21	13
HD 219828 ²	3.833±0.0013	7±0.5	0	0	0	2453898.63	...	1.7	27	2
HD 76700	3.97101±0.000203194	27.24±1.31	0.0616 ^{+0.0426} _{-0.0587}	12.3±54.3	45.6±53.8	2452655.1	...	1.35±4.21	35	1.13	1.34	0.23	0.99	2.80	9.84	6
HD 149143	4.07206±0.000320041	149.28±1.65	0.0123 ^{+0.0093} _{-0.0115}	-155.2±55.9	-150.9±55.9	2453413.1	0.027±0.005 ⁶	0.48±1.96	17	1.20	1.61	1.33	1.05	7.01	7.60	14
HD 102195 ³	4.1138±0.000557	63±2	0	0	0	2453895.96	...	6.1	59	3
51 PEG	4.2308±3.72905e-05	55.65±0.53	0.0069 ^{+0.0066} _{-0.0069}	54.1±72.3	85.1±72.3	2450404.4	-0.0045±0.0004 ⁶	0.27±0.91	256	1.09	1.18	0.47	1.03	6.61	6.76	6
GJ 674	4.6944±0.00182591	9.46±1.09	0.0700 ^{+0.0066} _{-0.0700}	0.5±71.2	77.6±71.1	2453823.784	...	3.55±0.55	32	0.35	0.46	0.04	1.13	0.21	0.55	15
HD 49674	4.94739±0.000974925	11.78±1.18	0.0495 ^{+0.0091} _{-0.0495}	-9.1±79.3	82.4±79.3	2452308.9	...	3.56±0.82	39	1.06	0.95	0.10	0.98	3.25	3.56	6
HD 109749	5.23921±0.000935533	28.49±1.12	0.0451 ^{+0.0250} _{-0.0451}	72.3±58.8	-155.1±55.8	2453426.3	...	0.31±1.10	20	1.21	1.28	0.28	0.99	12.04	10.30	14
HD 7924	5.39785±0.00096697	3.74±0.44	0.1186 ^{+0.0105} _{-0.0970}	25.0±55.6	62.1±54.8	2454096.65	0.35±0.07	2.59±0.22	93	0.83	0.78	0.03	1.05	0.61	0.88	16
HD 118203	6.13322±0.00129898	213.75±6.67	0.2943 ^{+0.0342} _{-0.0298}	-27.3±5.5	-2.9±4.8	2453351.2	0.14±0.016 ⁶	23.08±3.96	43	1.23	2.15	2.14	1.05	3.68	4.60	17
HD 68988	6.27699±0.0002195	184.63±4.69	0.1187 ^{+0.0246} _{-0.0216}	32.4±11.2	61.3±10.8	2452441.3	-0.065±0.005 ⁶	13.30±2.34	28	1.18	1.14	1.86	1.05	80.15	3.40	6
HD 168746	6.40398±0.000979461	28.41±1.38	0.0791 ^{+0.0541} _{-0.0791}	14.8±47.2	-147.2±47.3	2452510.8	...	0.41±1.62	16	0.93	1.04	0.25	0.99	20.31	12.40	6
HD 185269	6.83796±0.000119146	89.39±4.20	0.2758 ^{+0.0334} _{-0.0275}	173.3±6.4	47.3±6.4	2453795.0	...	7.70±2.10	30	1.28	1.88	0.94	1.04	19.34	4.20	8
HD 162020	8.42826±7.76104e-05	1808.84±5.26	0.2765 ^{+0.0023} _{-0.0025}	-151.2±0.3	68.3±1.0	2451672.02	...	11.02±3.43	46	0.78	0.74	15.00	0.98	148.00	0.76	19
GJ 176 ⁴	8.783±0.0054	4.1±0.52	0	0	0	2454399.8	...	2.5	57	4
HD 130322	10.7086±0.00184045	108.10±7.31	0.0068 ^{+0.0455} _{-0.0068}	128.3±93.9	-10.4±93.8	2452430.2	...	10.25±3.79	12	0.88	0.85	1.09	1.04	670.08	10.80	6
HD 108147	10.8984±0.00316767	24.60±3.62	0.5161 ^{+0.0979} _{-0.0966}	-54.4±14.0	-68.0±9.9	2452407.0	...	8.65±1.49	54	1.19	1.25	0.26	0.98	8.43	3.20	6
HD 4308	15.5646±0.0213556	4.20±0.34	0.0682 ^{+0.0547} _{-0.0682}	-166.9±60.6	-13.0±59.5	2453338.121	...	0.58±0.78	41	0.90	0.92	0.05	1.00	169.24	8.68	20
GJ 86	15.765±0.000382114	376.64±2.79	0.0416 ^{+0.0092} _{-0.0073}	-93.7±12.4	-76.8±12.0	2452199.4	-0.260±0.0029	10.67±1.62	42	0.77	0.80	3.91	1.05	6701.62	8.48	6
HD 99492	17.0495±0.000525091	8.39±0.98	0.0364 ^{+0.0089} _{-0.0364}	-138.6±93.6	-137.6±93.5	2452523.85	0.0035±0.0006 ⁶	3.96±0.51	86	0.86	0.76	0.11	0.96	692.89	1.80	21
HD 27894	18.0059±0.0163248	56.88±1.75	0.0240 ^{+0.0211} _{-0.0240}	131.3±66.5	-60.0288±66.5	2453344.278	...	4.48±1.07	20	0.75	0.90	0.62	1.02	3620.33	3.90	12
HD 33283	18.1801±0.00830584	24.48±2.41	0.4576 ^{+0.0656} _{-0.0569}	156.0±9.6	-60.0±7.4	2453560.0	...	0.27±0.94	24	1.24	1.20	0.33	0.99	203.12	3.20	8
HD 195019	18.2018±0.000595221	269.70±1.60	0.0017 ^{+0.0049} _{-0.0017}	-127.4±47.4	-175.5±47.3	2451844.0	...	10.50±1.22	154	1.07	1.38	3.69	1.05	4051.07	9.32	6
HD 102117	20.8210±0.01006465	10.20±0.91	0.0685 ^{+0.0529} _{-0.0640}	137.6±72.0	-9.5±72.5	2452931.7	...	0.57±1.73	44	1.11	1.26	0.17	0.95	3205.49	9.40	6
HD 17156	21.2178±0.00371004	279.88±8.43	0.6829 ^{+0.0106} _{-0.0106}	121.3±1.1	-156.7±1.2	2454111.21	...	3.68±0.64	34	1.24	1.63	3.20	1.04	19.10	8.00	10
HD 6434	21.9975±0.0127604	34.30±1.52	0.1589 ^{+0.0434} _{-0.0434}	155.4±15.8	-14.2±15.5	2451753.933	...	7.39±1.15	130	0.79	0.57	0.40	1.00	4393.14	6.85	22
HD 192263	24.3546±0.00507675	51.13±2.62	0.0256 ^{+0.0297} _{-0.0256}	-147.0±78.9	-56.7±78.9	2451867.6	...	6.99±1.31	31	0.81	0.77	0.64	1.02	14630.88	2.56	6
HD 117618	25.8221±0.0155045	12.25±1.70	0.3524 ^{+0.1583} _{-0.1192}	-105.6±22.9	-123.3±21.1	2452838.0	...	3.30±1.20	57	1.09	1.20	0.18	0.95	1435.34	5.68	6
HD 224693	26.732±0.0245934	39.73±1.54	0.0313 ^{+0.0236} _{-0.0313}	62.1±68.6	162.5±68.9	2453607.2	...	1.00±2.78	23	1.33	1.70	0.71	1.03	23506.41	2.00	8
HD 43691	36.9916±0.0350715	125.98±4.06	0.0897 ^{+0.0432} _{-0.0346}	91.3±26.2	16.7±24.9	2454046.7	...	10.35±2.58	36	1.38	1.92	2.49	1.04	42743.17	2.80	18
ρ Crb	39.8459±0.00917865	65.25±2.20	0.0476 ^{+0.0218} _{-0.0476}	-62.1±42.2	-172.6±42.5	2451181.1	...	0.65±2.79	26	1.00	1.28	1.09	1.03	166705.71	7.64	6
HD 45652	43.6896±0.105825	35.76±2.84	0.4339 ^{+0.0625} _{-0.0632}	83.2±12.8	77.7±10.2	2453692.66	...	8.38±2.20	45	0.83	1.04	0.47	1.01	12199.36	5.00	23
HD 107148	48.6168±3.59204	10.01±4.15	0.0279 ^{+0.1153} _{-0.0279}	126.5±90.8	-50.1±88.8	2452799.9	0.003±0.001 ²	3.53±1.04	35	1.14	1.12	0.21	0.96	122900.60	5.60	6

On the Eccentricity Distribution of Short-Period Single-Planet Systems

References: 1 Bouchy et al. (2005); 2 Melo et al. (2007); 3 Ge et al. (2006); 4 Forveille et al. (2009); 5 Maness et al. (2007); 6 Butler et al. (2006); 7 Zucker et al. (2004); 8 Johnson et al. (2006); 9 Winn et al. (2006); 10 Winn et al. (2009); 11 Lo Curto et al. (2006); 12 Moutou et al. (2005); 13 Pepe et al. (2004); 14 Fischer et al. (2006); 15 Ge et al. (2006); 16 Bonfils et al. (2007); 17 Howard et al. (2009); 18 da Silva et al. (2006); 19 da Silva et al. (2007); 20 Udry et al. (2002); 21 Udry et al. (2006); 22 Marcy et al. (2005); 23 Mayor et al. (2004); 24 Santos et al. (2008). Stellar radius and age estimations are obtained from the following sources with descending priority: 1, Takeda et al. (2007); 2, *nsted.ipac.caltech.edu*; 3, *exoplanet.eu*. τ_{circ} is calculated assuming $Q_* = 10^7$ and $Q_p = 10^7$

This paper has been typeset from a $\text{T}_\text{E}\text{X}/\text{L}_\text{A}\text{T}_\text{E}\text{X}$ file prepared by the author.